Journal of Power Sources 244 (2013) 189–195

Contents lists available at SciVerse ScienceDirect

Journal of Power Sources

journal homepage: www.elsevier.com/locate/jpowsour

Large discharge capacities at high current rates for carbon-coated $LiMnPO_4$ nanocrystalline cathodes

Hung-Cuong Dinh [a], Sun-il Mho [a], Yongku Kang [b], In-Hyeong Yeo [c,*]

[a] Division of Energy Systems Research, Ajou University, Suwon 443-749, Republic of Korea
[b] Division of Advanced Materials, Korea Research Institute of Chemical Technology, Daejeon 305-600, Republic of Korea
[c] Department of Chemistry, Dongguk University, Seoul 100-715, Republic of Korea

HIGHLIGHTS

- $LiMnPO_4$ nanoparticles of high crystallinity were synthesized.
- Carbon was coated by pyrolyzing sucrose wetted on the nanoparticle surfaces.
- The theoretical capacity of 171 $mAhg^{-1}$ was achieved at a rate of 0.1 C at 55 °C.

ARTICLE INFO

Article history:
Received 22 October 2012
Received in revised form
29 January 2013
Accepted 31 January 2013
Available online 14 February 2013

Keywords:
Nanocrystalline olivine cathode
Conductive coating
Hydrothermal method
Impedance analysis
Lithium ion battery

ABSTRACT

Nanocrystalline $LiMnPO_4$ particles approximately 100 nm in size are synthesized for use as a cathode material using a hydrothermal method. Small charge transfer resistances (R_{ct}) measured using electrochemical impedance spectroscopy (EIS) indicate that the particles are effectively coated with the conductive C layer by pyrolyzing sucrose in an inert atmosphere. The cathode composed of nanocrystalline C-coated $LiMnPO_4$ exhibits the largest specific capacities of 171 $mAhg^{-1}$ and 153 $mAhg^{-1}$ for the first cycle and 166 $mAhg^{-1}$ and 146 $mAhg^{-1}$ after 110 battery cycles at a rate of 0.05 C at 55 °C and 25 °C, respectively, with a degradation rate of 4 ± 1% after 110 battery cycles. The specific capacities are 165 $mAhg^{-1}$ and 142 $mAhg^{-1}$ for the first cycle at 55 °C for the nanoparticles with high crystallinity, even at high discharging current of 0.5 C and 5C, respectively. Diffusion coefficients of Li^+ in $LiMnPO_4$ (the fully discharged state) and in $MnPO_4$ (the fully charged state) are estimated to be 3.58×10^{-16} and 4.99×10^{-17} cm^2s^{-1}, respectively, from EIS in the low frequency region.

1. Introduction

Lithium ion batteries are one of the great successes in the development of electrochemical energy sources for use in modern portable electronic devices, and are expected to play an important part in large-scale applications for future electric vehicles, including hybrid vehicles [1–4]. A high level of safety, low environmental impact, low cost, and large power generation are the main requirements for the development of the most advanced energy storage systems. Olivine structured materials, such as $LiFePO_4$ and $LiMnPO_4$, have emerged as one of the most promising cathode materials for next generation Li batteries. These have a moderate theoretical capacity of approximately 170 $mAhg^{-1}$, good structural stability, low toxicity, and a relatively low cost [5–26]. $LiMnPO_4$ can offer a higher energy density than $LiFePO_4$, due to the higher Mn^{2+}/Mn^{3+} redox potential (4.1 V versus Li/Li^+) than the Fe^{2+}/Fe^{3+} (3.45 V) couple in the phosphate framework. Nevertheless, $LiMnPO_4$ has intrinsically poor electronic and ionic conductivities compared to $LiFePO_4$, when in the form of a cathode for Li ion battery applications. The extraction of Li^+ from $LiMnPO_4$ is both slow and incomplete, which pertains to the Jahn–Teller distortion experienced by Mn^{3+} that creates mechanical stress in the lattice and the large volumetric change between $LiMnPO_4$ and $MnPO_4$ during the charging/discharging processes [6–9]. Much effort has made to overcome the transport limitations and to improve the electrode performances by reducing the $LiMnPO_4$ particle sizes, by minimizing the defect concentration, and by coating with conductive carbon materials [6–26]. Individual nanocrystalline particles have the benefit of increasing the battery capacity and enhancing the charge/discharge rate, due to the resulting increase in the specific surface area and decrease in diffusion length for Li^+ ions. In order to improve the intrinsic problem of low ion

* Corresponding author.
E-mail address: ihyeo@dgu.ac.kr (I.-H. Yeo).

0378-7753/$ – see front matter © 2013 Elsevier B.V. All rights reserved.
http://dx.doi.org/10.1016/j.jpowsour.2013.01.191

diffusivity, it is essential to minimize defect concentration as well as reducing the crystallite size [10–17]. Hydrothermal synthesis is an effective method for obtaining highly crystalline materials with well-defined morphologies. Even though this method is a low temperature synthetic procedure, it is carried out under high pressure, which is considered to be a crucial factor in the production of highly crystallized nanoparticles [17–20]. The particle size and morphology can be controlled by a careful choice of surfactants, solvents, and reaction parameters in the hydrothermal synthesis. In addition, considerable efforts have been made to improve the conductivity and the charge/discharge rate of $LiMnPO_4$ by surface coating [21–26]. Carbon coating on nanosized $LiMnPO_4$ particle surfaces by pyrolyzing organic precursors under reducing conditions has been shown to improve electrode conductivity [22]. The kinetics of Li^+ ion movement within electrode lattices and transport through the interfaces of the cell components is a critical factor for identifying the discharge and charge rates [27–29].

In this work, nanocrystalline and micro-structured $LiMnPO_4$ particles with various sizes and shapes were prepared using a hydrothermal method. Moreover, in order to increase the charge transport kinetics, these particles were coated with C, formed by pyrolysis of sucrose. The electrochemical performances of the C-coated $LiMnPO_4$ crystalline nanoparticles and microballs were examined in terms of cycle stability and discharge capacity when acting as cathode materials in Li ion batteries. The conductivity and accessibility of the Li ion through the interface and electrode materials is a critical factor for determining discharge and charge rates. In order to obtain a better understanding of Li^+ transport in the battery, we performed ac impedance measurements during the charging and discharging processes of the C-coated $LiMnPO_4$ nanoparticle cathodes, and the charge transfer resistances (R_{ct}) and Li ion diffusion through the crystalline $LiMnPO_4$ particles were estimated. In the present study, the analysis and comparison of the crystal structure, morphology, impedance values, and electrochemical properties of the conductive C-coated $LiMnPO_4$ crystals were addressed.

2. Experimental

2.1. Material preparation

All chemicals and materials were obtained from Sigma–Aldrich Corporation and used without further purification. All aqueous solutions were prepared with ultra-pure water deionized by a Millipore Milli-Q system (18 $M\Omega cm^{-1}$). $LiMnPO_4$ crystalline particles were synthesized using a hydrothermal method from a stoichiometric mixture of the starting materials of LiOH, manganese ion salts [$Mn(NO_3)_2{\cdot}6H_2O$, $Mn(CH_3CO_2)_2{\cdot}4H_2O$, $MnCl_2{\cdot}4H_2O$, or $MnSO_4.4H_2O$], and H_3PO_4 (3:1:1 M ratio). L-ascorbic acid ($C_6H_8O_6$, 99%) was added to the mixture of the starting materials as an antioxidant (Mn^{2+}:$C_6H_8O_6$ = 4:1 M ratio). Ethylene glycol was added into the aqueous solution to disperse the inorganic salts (1:1 volume ratio) [17]. Citric acid, hexadecyltrimethyl ammonium bromide (CTAB), or a block copolymer of poly(ethylene glycol)-block-poly(propylene glycol)-block-poly(ethylene glycol) (Pluronic P123) was added as a surfactant to control the particle growth and surface morphology. The resulting solution was transferred to a 125 ml Teflon-lined stainless steel autoclave and heated at 180 °C for 12 h. After the hydrothermal reaction was complete, the precipitate was washed thoroughly and dried at 80 °C.

In order to form a smooth C coating on the surface of the $LiMnPO_4$ particles, $LiMnPO_4$ powder was dispersed in a sucrose solution, and the subsequently formed coated $LiMnPO_4$ particles were heated at 600 °C in a N_2 atmosphere to completely pyrolyze the sucrose to C (C-coated $LiMnPO_4$).

2.2. Characterization

The crystalline structures of the $LiMnPO_4$ samples were identified using an X-ray diffractometer (XRD, Rigaku, DMAX-2200PC, Japan) that utilized Cu-Kα radiation (λ = 1.54056 Å). Data were collected over the 2θ range from 10° to 100° for 4 s in each 0.02° step at ambient temperature. The structural parameters were refined by using the Rietveld program FULLPROF [30]. Scanning electron microscopy (FESEM JSM-6700F and SEM JSM-6380, JEOL, Japan) was used to examine the morphology of the particles. The specific surface areas of $LiMnPO_4$ materials were measured by the Brunauer, Emmett, and Teller (BET, ASAP2010, Micromeritics Inc) method from the nitrogen adsorption isotherm, after the samples were vacuum dried at 200 °C for 5 h. The amount of C coated on the particles was analyzed using thermogravimetric analysis (TGA, Nezsch STA 409 PC/PG).

The lithium batteries were assembled in a coin-type (CR2032) cell with C-coated $LiMnPO_4$ cathodes of various morphologies, in a dry room. The mixtures of acetylene black (AB), polyvinylidene fluoride (PVDF) binder, and the C-coated $LiMnPO_4$ were dissolved in N-methyl-2-pyrrolidone (NMP). The resulting slurry was spread on a thin sheet of Al foil (Doctor Blade method), pressed, and dried in a vacuum. Li foil was used as an anode. The electrolyte used was 1 M $LiPF_6$ in a 1:1 (v/v) mixture of ethylene carbonate (EC) and dimethyl carbonate (DMC). The Li batteries were cycled with a constant current mode (galvanostatically) in a potential range of 2.0–4.4 V using a multichannel battery test system (Maccor Series 4000, USA). The constant current-constant voltage (CC–CV) mode was used for the charge process to maximize the reversible capacity and coulombic efficiency. The cells were charged with a C/20 rate to 4.4 V, kept at 4.4 V until the current dropped to 20% of the initial value (a C/100 rate), and then discharged to 2.0 V at the specific rate. Cyclic voltammograms (CV) were recorded using a multi-electrochemical analyzer system (Bio-Logic VSP 0417) at a scan rate of 0.05 mV s^{-1} in a potential limit from 2.0 to 4.8 V for a Li coin cell with a C-coated nanocrystalline $LiMnPO_4$ cathode. All electrochemical measurements were performed at both 25 °C and 55 °C. Electrochemical impedance measurements (Schlumberger SI 1260 with a SI 1268 interface) were performed by applying an ac signal in the frequency range of 10 mHz–1 MHz with 5 mV_{p-p} after the 0.05 C cyclic initialization of the battery.

3. Results and discussion

3.1. Structural and morphological characterization

The size and morphology of $LiMnPO_4$ particles were examined using SEM. Fig. 1 shows the obtained images of the nanoparticles and the microball-shaped $LiMnPO_4$ that were synthesized using the hydrothermal method. Uniform particles with a controlled size and morphology were achieved. The surfactant added with the starting ingredients plays a critical role in determining the morphology of the $LiMnPO_4$, by effectively controlling the particle growth [17,18]. The well-dispersed individual nanosized $LiMnPO_4$ crystals formed in the presence of the large surfactants, such as CTAB or P123, displayed particle shape (100 nm) or rod shape (~1-μm long), as shown in Fig. 1a and b. On the other hand, the smaller molecular surfactant, citric acid, could adsorb onto the particle surface during particle growth, and in turn could organize the nanoscale building blocks into the micron-sized individual $LiMnPO_4$ balls (~10 μm in diameter) via a self-assembly process, as shown in Fig. 1c. The morphologies of nanocrystalline $LiMnPO_4$ particles that were coated with C by heating the $LiMnPO_4$ particles soaked in sucrose solutions were seen to maintain their original shapes (Fig. 1d).

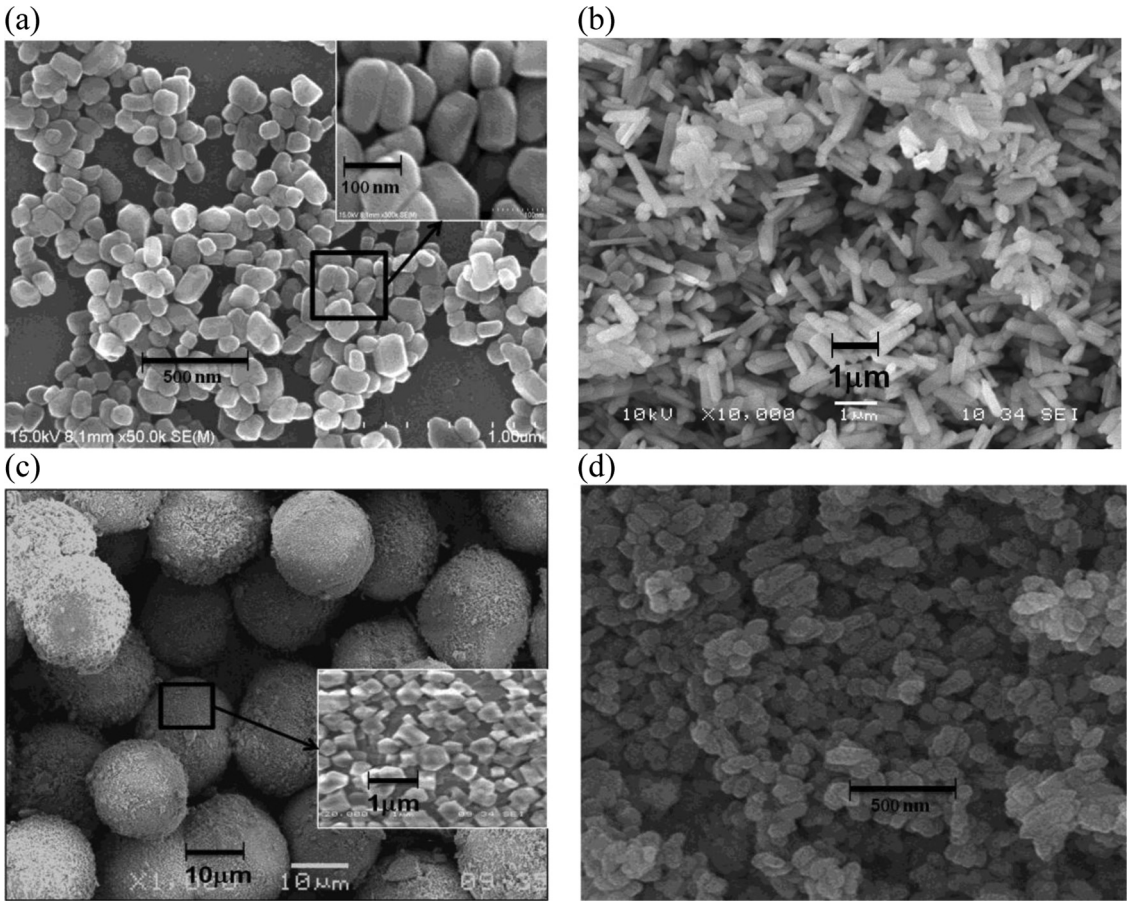

Fig. 1. SEM images of the different $LiMnPO_4$ powders; (a) nanosized grain-shape crystals, (b) rod-shape crystals, (c) micron-sized ball-shape crystalline $LiMnPO_4$ with nanocrystals on the surface, and (d) C-coated nanocrystalline particles of (a).

The specific surface areas determined by BET measurement of $LiMnPO_4$ nano-crystalline particles (~100 nm), rod-shape (~1-μm long) crystals, and microball-shaped (~10 μm dia.) microstructures were estimated to be 63.4, 9.56, and 6.21 $m^2\ g^{-1}$, respectively. The specific surface area considerably decreases with increasing the particle size, and the smallest $LiMnPO_4$ nanocrystalline particle has the largest specific surface area.

The XRD patterns of the $LiMnPO_4$ particles with various shapes are shown in Fig. 2A. All diffraction peaks are well matched with those of the standard pattern of $LiMnPO_4$ (ICSD No. 97763). The diffraction peaks of the various morphologies of the $LiMnPO_4$ particles prepared by the hydrothermal method can be seen to be intense, which indicates that the nanostructures are well crystallized. The observed, calculated, and difference XRD patterns from the Rietveld refinement for the as-synthesized nanocrystalline $LiMnPO_4$ are shown in Fig. 2B. All diffractions for the nanocrystalline $LiMnPO_4$ in the powder XRD patterns were indexed by an orthorhombic structure with the *Pnma* space group with $a = 10.450$ Å, $b = 6.102$ Å, $c = 4.746$ Å, and $v = 0.30263\ nm^3$. The final atomic coordinates, isotropic temperature factors, and agreement factors from this structural model are listed in Table 1. Each orthorhombic unit cell contains four formula units and each PO_4 tetrahedron is surrounded by four MnO_6 octahedra (three corner-sharing and one edge-sharing), with Li^+ ions occupying the large open channels running parallel to the *b* axis. Since the Li^+ transport is one-dimensional in the olivine structure, it is essential to minimize defect concentration and to increase the crystallinity. The Li^+ mobility was simulated to be high in the tunnels along the [010] direction only, with Li^+ hopping between tunnels being highly unlikely in the olivine structure [9,11,27,30–32]. The XRD peak positions and intensities of the C-coated $LiMnPO_4$ were the same as the genuine peaks of the pristine $LiMnPO_4$, which indicates that the C coating processes did not cause any structural changes in the $LiMnPO_4$ particles (data not shown).

3.2. Electrochemical performance of the C-coated $LiMnPO_4$ powders as cathodes

After assembling coin-type Li cells with the cathodes composed of the prepared $LiMnPO_4$ powders, the electrochemical performances were evaluated using a battery test system. For the cathode of CR2032 type coin cell, the loadings of $LiMnPO_4$ nanocrystals (~100 nm), rod-shape (~1-μm long) crystals, and microball-shaped (~10 μm dia.) microstructures were 4.65, 3.96, and 3.59 mg, respectively. Fig. 3 shows the voltage–capacity profiles during the first charge/discharge cycle at a constant current rate of C/20 for the various C-coated (10 wt%) $LiMnPO_4$ crystals. The charge/discharge profile of the $LiMnPO_4$ nanocrystals maintained the characteristic shape with voltage plateaus at around 4.1 V. All the curves showed reversible Li extraction/insertion during the charging/discharging processes, with varying specific capacities. The charge and discharge profile shown in Fig. 3 demonstrates that the cathode consisting of the smallest $LiMnPO_4$ nanoparticles (100 nm in size) delivered the highest specific capacity of 153 $mAhg^{-1}$. The cathodes made from the rod-shaped crystalline and the microball-shaped $LiMnPO_4$ had capacity values of approximately 116 $mAhg^{-1}$ and 36 $mAhg^{-1}$,

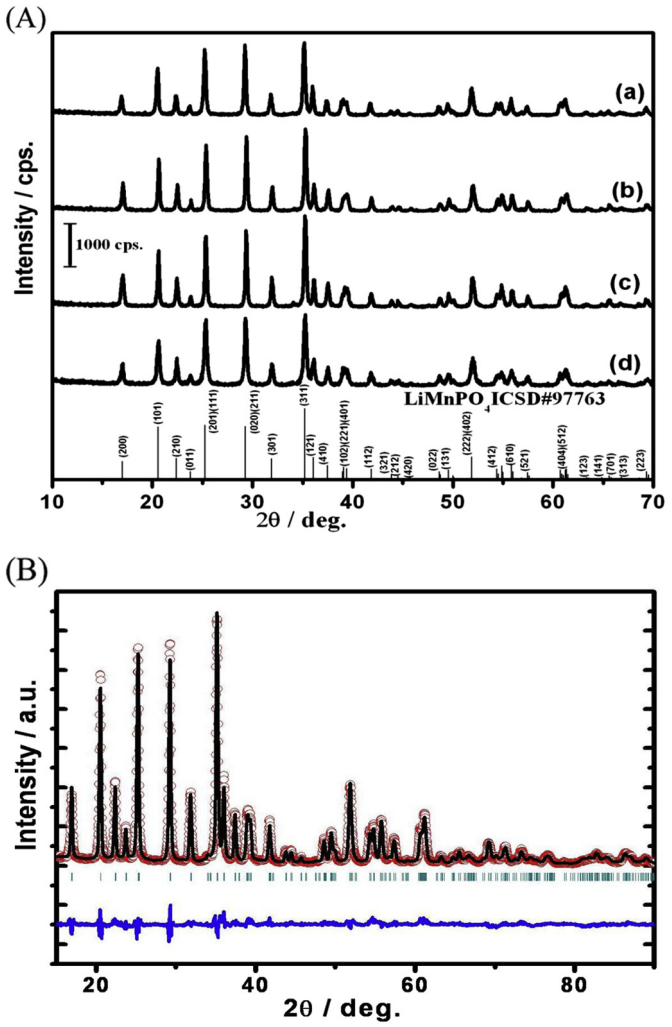

Fig. 2. (A) The XRD spectra of the different $LiMnPO_4$ powders; (a) nanosized grain-shape crystals, (b) rod-shape crystals, (c) micron-size ball-shaped $LiMnPO_4$, and (d) C-coated nanocrystalline particles of (a). (B) Observed (o), calculated (—), and difference (bottom line) powder X-ray Rietveld profiles for nanocrystalline $LiMnPO_4$. The vertical tick marks below the profile show the Bragg positions.

respectively. The nanocrystalline particle (100 nm in size) cathodes exhibited the highest specific capacity resulting from the increased surface area and the reduced diffusion path lengths for Li ions in the material. The low specific capacity value for the micron-sized particles is considered to be caused by the adverse effect of the low conductivity of the pristine material itself. In order to overcome the low intrinsic electronic conductivity and slow Li diffusion kinetics within the cathode material, particle size reduction is essential for

Table 1
Final atomic coordinates, isotropic temperature factors, and agreement factors from the structural model for $LiMnPO_4$.

Space group: *Pnma* $a = 10.450$ Å, $b = 6.102$ Å $c = 4.746$						
$R_p = 8.34\%$	$R_{wp} = 11.1\%$	$R_{exp} = 11.66\%$	$\chi^2 = 0.90(6)$			
Atom	Site	*g*	*x*	*y*	*z*	B (Å^2)
Li	4a	0.50	0	0	0	0.992
Mn	4c	0.50	0.281	0.250	0.971	1.742
P	4c	0.50	0.093	0.250	0.409	1.533
O	4c	0.50	0.095	0.250	0.725	1.093
O	4c	0.50	0.457	0.250	0.223	1.093
O	8d	1.00	0.160	0.050	0.281	1.093

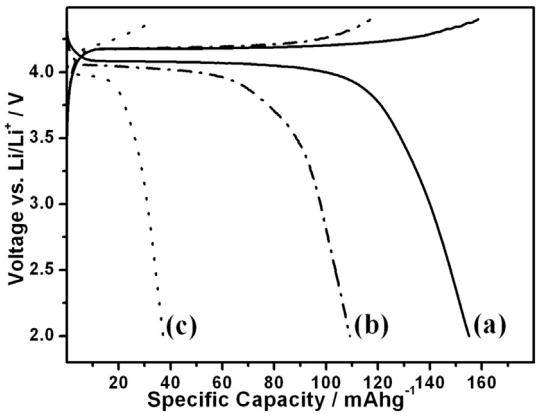

Fig. 3. The first charge and discharge curves recorded at a 0.05 C rate for the cathode composed of the C-coated (10 wt%) (a) nanosized grain-shape $LiMnPO_4$, (b) rod-shape $LiMnPO_4$, and (c) microball-shaped $LiMnPO_4$ crystals.

improving the rate performance. In addition, the smaller the particle is, the more densely the particles can be packed with smaller interstitial volumes in the cathode. High packing degree with small void volume results in high tap density. High tap density leads to a high volumetric specific capacity. The tap densities of $LiMnPO_4$ nanocrystals (~100 nm), rod-shape (~1-μm long) crystals, and microball-shaped (~10 μm dia.) microstructures were 1.20, 1.07, and 0.96 gcm^{-3}, respectively. As the nanocrystalline $LiMnPO_4$ possesses the highest tap density (1.20 gcm^{-3}) among the various morphologies, a high volumetric specific capacity (183.6 mAhg cm^{-3}) was achieved.

Cyclic voltammograms (CVs) of Li batteries with a cathode composed of nanocrystalline $LiMnPO_4$ powders, in the potential range of 2.0–4.8 V at 25 °C and 55 °C are shown in Fig. 4. A reduction-peak appears around 3.98 V and an oxidation-peak around 4.30 V in the CVs obtained at 25 °C. The oxidation current and reduction current seem to be symmetric, which indicates reversibility of the redox reaction. At an elevated temperature (55 °C), the peak currents increased with decreased peak separation ($\Delta E(p_a - p_c) = 0.21$ V). The increased intensity of the pair of peaks would be ascribed to the enhanced mobility of the lithium ion, which results from the increased lithium ion diffusion rate and the accelerated redox reaction of Mn^{2+}/Mn^{3+}. According to these CVs, voltage plateaus around 4.0–4.2 V are expected in the voltage–capacity profile during the discharge/charge cycles. The

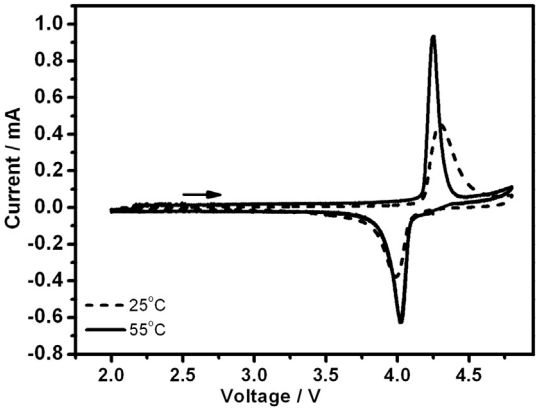

Fig. 4. Cyclic voltammograms of a Li battery assembled with a cathode consisting of nanocrystalline C-coated $LiMnPO_4$ at (a) 25 °C and (b) 55 °C. The scan rate was 0.05 mV s^{-1}.

typical redox potential of Mn^{2+}/Mn^{3+} in olivine manganese phosphate is 4.1 V versus Li/Li^+.

As shown in Fig. 5, the charge/discharge cycle performances under various discharge rates, ranging from C/20 to 10 C with five cycles at each rate, were tested for the Li batteries composed of the C-coated (10 wt%) $LiMnPO_4$ nanocrystals both at 25 °C and at 55 °C. The flat charging–discharging plateau at around 4.1 V expanded to greater values of capacity at the lower C rates and this plateau usually disappeared at the high C rates. The first charge/discharge curves recorded at each discharging rate at 25 °C and 55 °C are shown in Fig. 5a and b, respectively. The specific capacities generally decreased as the discharge rate increased for the cathodes. The discharge plateau-voltage decreased from 4.1 V to 3.7 V as the current increased from C/20 to 10 C, at 25 °C, and the plateau became short with increasing discharge rate and more than half of the capacity comes from the slope between 3.9 and 2.0 V. The first discharge capacity at the C/20 rate is 154 $mAhg^{-1}$, and the discharge capacities at various discharging rates are 152 $mAhg^{-1}$ at C/10, 140 $mAhg^{-1}$ at C/2, 128 $mAhg^{-1}$ at 1 C, 123 $mAhg^{-1}$ at 2 C, 111 $mAhg^{-1}$ at 5 C, and 92 $mAhg^{-1}$ at 10 C. However at 55 °C, the voltage plateau extended to large values of capacity with a small polarization loss at fairly high plateau-voltages above 3.9 V. At 55 °C, the first discharge capacity at the C/20 rate is the highest value, 171 $mAhg^{-1}$, with a prolonged plateau at 4.1 V, which is approximately the theoretical value. The discharge capacities at various discharging rates at 55 °C are 169 $mAhg^{-1}$ at C/10, 165 $mAhg^{-1}$ at C/2, 159 $mAhg^{-1}$ at 1 C, 149 $mAhg^{-1}$ at 2 C, 142 $mAhg^{-1}$ at 5 C, and 128 $mAhg^{-1}$ at 10 C. This is the best performance reported to date at these rates [14,15,22–25]. The capacity retention capability was estimated by returning back to the initial rate of C/20 as the last step after testing 35 battery cycles at rates from C/20 to 10 C, five cycles at each rate. The specific capacities returned to a level close to the initial states of C/20, although the specific capacity decreased with increased rates as indicated during the 35 cycles, either at 25 °C or 55 °C.

The amount of the conductive C coated on the $LiMnPO_4$ nanoparticles is an important factor that needs to be controlled. The battery performances were also tested for the $LiMnPO_4$ nanocrystals coated with different amounts of C up to 20 wt%. The cathode composed of the $LiMnPO_4$ nanoparticles with 10 wt% C coating exhibited larger specific capacities than those with other amounts of the coating (data not shown).

Long-term cycle stability at the rate of C/20 and at a higher discharge current rate of C/2 for the cathodes made of nanocrystalline C-coated $LiMnPO_4$ particles were investigated. Fig. 6 contains the discharge specific capacities of 110 completed charge/discharge cycles at both 25 °C and 55 °C of the batteries assembled with cathodes composed of nanocrystalline C-coated $LiMnPO_4$ particles, which revealed excellent cycling stability with a degradation rate of approximately 3–5%. The largest specific

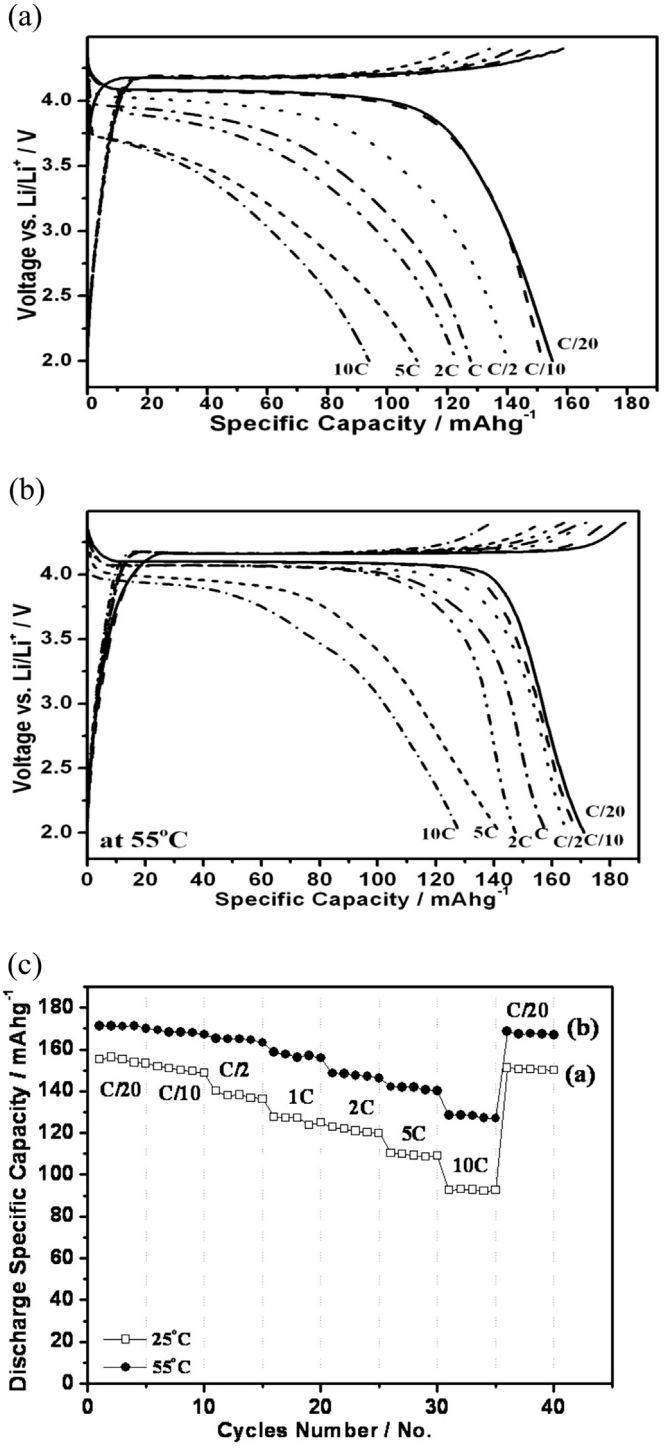

Fig. 5. Cycle stability test carried out by sequentially increasing the discharge rates from 0.05 C to 10 C for the nanocrystalline C-coated $LiMnPO_4$ at both 25 °C and 55 °C. The cells were charged at a constant current rate of 0.05 C to 4.4 V and kept at 4.4 V until 0.01 C. The first charge–discharge curves at each rate are displayed at (a) 25 °C and (b) 55 °C. (c) Five cycles at each discharge rate were recorded and the discharge rate was returned to the initial rate of 0.05 C for the last step.

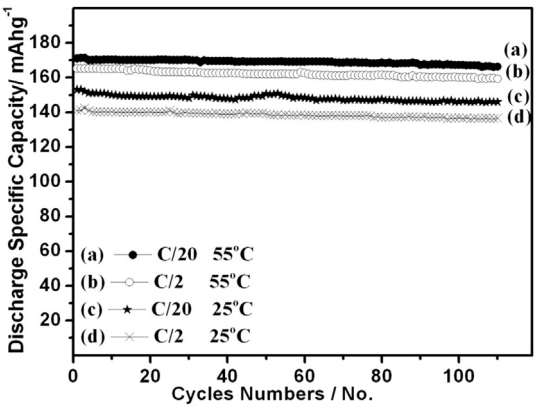

Fig. 6. Long-term stability test over 100 charge–discharge cycles both at 55 °C (a & b) and 25 °C (c & d). Specific capacities obtained at the rates of 0.05 C (a & c) and 0.5 C (b & d) for Li batteries assembled with cathodes of the nanocrystalline C-coated $LiMnPO_4$.

capacities of the cathode composed of nanocrystalline C-coated (10 wt%) $LiMnPO_4$ were 171 $mAhg^{-1}$ and 153 $mAhg^{-1}$ at 55 °C and 25 °C, respectively for the first cycle, and 166 $mAhg^{-1}$ and 146 $mAhg^{-1}$ after 110 battery cycles at a rate of 0.05 C. The specific capacities were 165 $mAhg^{-1}$ and 141 $mAhg^{-1}$ for the first cycles at 55 °C and 25 °C, respectively, even at a high discharging current of 0.5 C. Decreasing the crystallite size to sub-micron or nanometer size is important for enhancing electrochemical performance, both by reducing the Li^+ transport path lengths and by reducing the mechanical lattice strain upon Li^+ insertion/extraction. In addition, morphological control of nanocrystalline materials is very important, since many of the properties are dependent on the shape. The different morphologies of the nanosized $LiMnPO_4$ particles prepared through various approaches also affected the charge/discharge behavior of the C-coated $LiMnPO_4$ cathode, which is an interesting phenomenon that is worth investigating in the future.

Impedance measurements can probe and detect Li^+ ion movement within electrode lattices and electrode–electrolyte interfaces at various charged states of the battery. In order to understand the kinetics of the C-coated $LiMnPO_4$ nanoparticles, we performed ac impedance measurements during the charging and discharging processes. During the reversible charge/discharge of the $LiMnPO_4$ cathodes, the Li ion is extracted from or inserted into the lattices producing a $Li_{1-x}MnPO_4$ composition with $0 \leq x \leq 1$. Fig. 7 shows four Nyquist plots of the impedance data obtained for the Li batteries that were assembled with the C-coated nanocrystalline $LiMnPO_4$ cathode during the discharging process, when they are fully charged (100%; C100), partially-discharged (60%; C60 and 30%; C30), and completely discharged (0%; C0). The impedance values changed continuously depending on the state of charge (SoC) of the same battery. From the real part of the graph (Z_{real}, in-phase impedance value; *x*-axis), the series ohmic resistances (R_s) and charge transfer resistances (R_{ct}) can be estimated [27–29]. The Z_{real} value at the highest frequency (R_s) corresponds to the total cell resistance of the electrodes, electrolyte, separator, and electrical contacts. The value of R_s was approximately 5 Ω for all the Li cells assembled with the cathodes of C-coated $LiMnPO_4$ nanocrystals. The diameter of the semicircle in the high frequency range is related to R_{ct} at the interface of the crystalline $LiMnPO_4$ particles. The values of R_{ct} are estimated to be in the range of 28–45 Ω for the fully charged to completely discharged states. There is an increasing trend in the value of R_{ct} from the fully charged state to the completely discharged state during both the charging and the discharging process. The value of R_{ct} for the fully charged state is somewhat smaller than that of the completely discharged state. Charge transfer through the electrode–electrolyte interface apparently becomes easier with the charged (delithiated) state. Coating with C can effectively increase the electrode conductivity, improve the surface chemistry of the active material, and protect the electrode from direct contact with electrolyte, leading to enhanced cycle lifetime of the batteries. This coating, in combination with nanotechnology, provides good conductivity as well as fast Li ion diffusion, thus resulting in good rate capabilities.

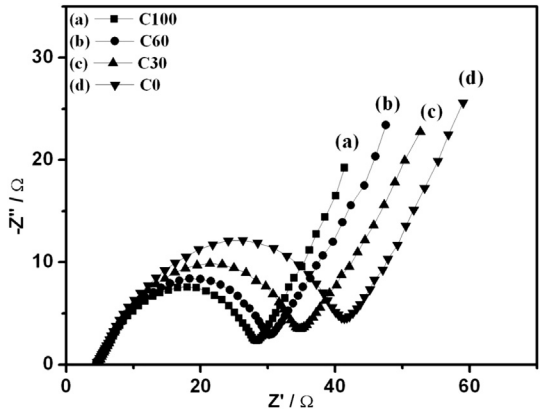

Fig. 7. Impedance spectra (Nyquist plots) for the Li battery assembled with the nanocrystalline C-coated $LiMnPO_4$ (a) at fully charged state (SoC 100%; C100), (b) at SoC 60% (C60), (c) at SoC 30% (C30), and (d) at fully discharged state (SoC 0%; C0). Frequency range: 1.0 Hz–1.0 MHz.

In addition, the impedance data in the low frequency region are expected to be dominated by Warburg impedance, which is associated with Li ion diffusion through the crystalline $LiMnPO_4$ particles. A straight line with an angle of 45° with respect to the real (Z′) axis was observed in the low frequency region (1.0–10 Hz) of the Nyquist plot (Fig. 7). The diffusion coefficient (D_{Li+}) of $LiMnPO_4$ was calculated using the equation proposed by Ho et al. [28,29].

$$D_{Li+} = 1/2[(V_m/SFA)(dE/dx)]^2 \quad (1)$$

where V_m is the molar volume of $LiMnPO_4$ (45.66 $cm^3\ mol^{-1}$), *S* is the contact area between the electrolyte and the cathode (626 cm^2), *F* is Faraday's constant (96485 C mol^{-1}), d*E*/dx is the variation of the open-circuit voltage accompanying the change in the Li content (*x*) in the crystalline Li_xMnPO_4, and *A* is estimated from the plot of the real (Z′) or imaginary (Z″) part of the Warburg impedance versus $\omega^{-1/2}$ ($Z_\omega = A\omega^{-1/2} - jA\omega^{-1/2}$). The value for D_{Li+} calculated for the initial fully charged state was 4.99×10^{-17} cm^2s^{-1}, which is considered to be the value for Li_0MnPO_4 nanocrystals. In the fully discharged region where the phase transition to $LiMnPO_4$ is complete, D_{Li+} was estimated to be 3.58×10^{-16} cm^2s^{-1}. Values of D_{Li+} are dependent on the state of charge and on the composition of Li_xMnPO_4; the values for D_{Li+} values for the partially-discharged C60 and C30 states were 8.55×10^{-21} and 3.33×10^{-18} cm^2s^{-1}, respectively. In the monophase regions of the fully charged ($MnPO_4$) and fully discharged ($LiMnPO_4$) states of the cathode, the values for D_{Li+} are larger than those for the intermediate states (binary phases) of charge, which is similar to the $LiFePO_4/FePO_4$ system [27]. It is speculated that the somewhat smaller value of D_{Li+} for the of fully charged $MnPO_4$ state than that for the fully discharged $LiMnPO_4$ state are due to the heavy polaronic holes on the Mn^{3+} sites and that the slower lithium diffusion kinetics for the binary phases is caused by the interface strain between $LiMnPO_4$ and $MnPO_4$ [14]. Further in depth investigations of the diffusion process, migration, and charge transfer mechanism are currently in progress.

4. Conclusion

In order to overcome the inherently low conductivity of the $LiMnPO_4$ cathode material, the crystallite particle size of $LiMnPO_4$ was minimized and these nanoparticles were coated with conductive C by pyrolyzing sucrose. Particles of $LiMnPO_4$ with controlled morphologies and sizes were synthesized using a hydrothermal process. Nanocrystalline $LiMnPO_4$ particles with grain- and rod-shapes were formed in the presence of large surfactants and $LiMnPO_4$ microballs were synthesized by using a small surfactant. The nanosized particles had large surface-to-volume ratios, which is desirable for the Li ions to have sufficient access to $LiMnPO_4$ during the charge/discharge cycling of rechargeable batteries.

The nanocrystalline C-coated $LiMnPO_4$ (100 nm in size) exhibited excellent electrochemical performance, showing the full theoretical specific capacity of $LiMnPO_4$ at a rate of 0.1 C or lower (169 $mAhg^{-1}$ and 171 $mAhg^{-1}$ at 0.1 C and 0.05 C rates, respectively) at 55 °C. The nanocrystalline C-coated (10 wt%) $LiMnPO_4$

exhibited the best cycle performance with the largest specific capacity, with the capacity fading by 3–5%. We believe that the high crystallinity of the $LiMnPO_4$, low lattice defects, and short diffusion lengths in the particles, enhanced the kinetics by improving the ion movement through the b channel of the olivine structure. The values of R_{ct} estimated from the impedance analysis were extremely small due to complete coverage of the particles with the conductive material. The values of D_{Li+} calculated for the fully charged state (Li_0MnPO_4) and the fully discharged state ($LiMnPO_4$) were 4.99×10^{-17} and 3.58×10^{-16} cm^2s^{-1}, respectively.

Acknowledgments

This research was performed as a cooperation project supported by the Korea Research Institute of Chemical Technology. This work was partly supported by the National Research Foundation of Korea (2009-0094046).

References

[1] J.B. Goodenough, J. Solid State Electrochem. 16 (2012) 2019–2029.
[2] J.W. Fergus, J. Power Sources 195 (2010) 939–954.
[3] J. Li, C. Daniel, D. Wood, J. Power Sources 196 (2011) 2452–2460.
[4] M. Armand, J.-M. Tarascon, Nature 451 (2008) 652–657.
[5] A.K. Padhi, K.S. Nanjundaswamy, J.B. Goodenough, J. Electrochem. Soc. 144 (1997) 1188–1194.
[6] A. Yamada, S.-C. Chung, J. Electrochem. Soc. 148 (2001) A960–A967.
[7] M. Yonemura, A. Yamada, Y. Takei, N. Sonoyama, R. Kanno, J. Electrochem. Soc. 151 (2004) A1352–A1356.
[8] C. Delacourt, P. Poizot, J.-M. Tarascon, C. Masquelier, Chem. Mater. 16 (2004) 93–99.
[9] C.A.J. Fisher, V.M.H. Prieto, M.S. Islam, Chem. Mater. 20 (2008) 5907–5915.
[10] J. Kim, K.-Y. Park, I. Park, J.-K. Yoo, D.-H. Seo, S.-W. Kim, K. Kang, J. Electrochem. Soc. 159 (2012) A55–A59.
[11] R. Malik, D. Burch, M. Bazant, G. Ceder, Nano Lett. 10 (2010) 4123–4127.
[12] S.K. Martha, O. Haik, E. Zinigrad, I. Exnar, T. Drezen, J.H. Miners, D. Aurbach, J. Electrochem. Soc. 158 (2011) A1115–A1122.
[13] C. Delacourt, P. Poizot, S. Levasseur, C. Masquelier, Electrochem. Solid State Lett. 9 (2006) A352–A355.
[14] D. Choi, D. Wang, I.-T. Bae, J. Xiao, Z. Nie, W. Wang, V.V. Viswanathan, Y.J. Lee, J.-G. Zhang, G.L. Graff, Z. Yang, J. Liu, Nano Lett. 10 (2010) 2799–2805.
[15] D. Wang, H. Buqa, M. Crouzet, G. Deghenghi, T. Drezen, I. Exnar, N.-H. Kwon, J.H. Miners, L. Poletto, M. Grätzel, J. Power Sources 189 (2009) 624–628.
[16] A.V. Murugan, T. Muraliganth, A. Manthiram, J. Electrochem. Soc. 156 (2009) A79–A83.
[17] H.-C. Dinh, S.-i. Mho, I.-H. Yeo, Electroanalysis 23 (2011) 2079–2086.
[18] M.K. Devaraju, I. Honma, Adv. Energy Mater. 2 (2012) 284–297.
[19] B. Ellis, W.H. Kan, W.R.M. Makahnouk, L.F. Nazar, J. Mater. Chem. 17 (2007) 3248–3254.
[20] A.V. Murugan, T. Muraliganth, P.J. Ferreira, A. Manthiram, Inorg. Chem. 48 (2009) 946–952.
[21] H. Li, H. Zhou, Chem. Commun. 48 (2012) 1201–1217.
[22] T.N.L. Doan, I. Taniguchi, J. Power Sources 196 (2011) 1399–1408.
[23] S.-M. Oh, S.-W. Oh, C.-S. Yoon, B. Scrosati, K. Amine, Y.-K. Sun, Adv. Funct. Mater. 20 (2010) 3260–3265.
[24] Z. Qin, X. Zhou, Y. Xia, C. Tang, Z. Liu, J. Mater. Chem. 22 (2012) 21144–21152.
[25] D. Rangappa, K. Sone, Y. Zhou, T. Kudo, I. Honma, J. Mater. Chem. 21 (2011) 15813–15818.
[26] Z. Bakenov, I. Taniguchi, J. Power Sources 195 (2010) 7445–7451.
[27] M. Park, X. Zhang, M. Chung, G.B. Less, A.M. Sastry, J. Power Sources 195 (2010) 7904–7929.
[28] C. Ho, I.D. Raistrick, R.A. Huggins, J. Electrochem. Soc. 127 (1980) 343–350.
[29] H. Joachin, T.D. Kaun, K. Zaghib, J. Prakash, J. Electrochem. Soc. 156 (2009) A401–A406.
[30] J.R. Carvajal, FULLPROF 2000: A Rietveld Refinement and Pattern Matching Analysis Program, Laboratoire Leon Brillouin (CEA-CNRS), France, 2008.
[31] S.P. Ong, V.L. Chevrier, G. Ceder, Phys. Rev. B 83 (2011) 075112–075117.
[32] M. Thackeray, Nat. Mater. 1 (2002) 81–82.